FOSSEE, IIT Bombay
OpenFOAM Case Study Project
June 23, 2026

FOSSEE CFD-OpenFOAM Semester Long Internship Spring 2026 on FSI of Rotating Porous Square Cylinder Using Continuous Forcing Immersed Boundary Method

Prajwol Bohara[1],Manjil Sitoula[2],Anirudha Kulkarni[3]

[1]Department of Automobile and Mechanical Engineering, IOE Thapathali Campus, Institute of Engineering, Tribhuvan University, Nepal
[2]Research Assistant,FOSSEE, IIT Bombay
[3]Assistant Professor, Department of Mechanical Engineering Pandit Deendayal Energy University, Gandhinagar

Abstract

This case study presents a comprehensive numerical study of flow past a rotating porous square cylinder using the continuous forcing immersed boundary method. A finite volume approach combined with the immersed boundary method (IBM) and moving boundary treatment is employed to obtain the numerical results. The investigation covers steady flow regimes ($10 \leq Re \leq 40$) with different values of permeability (Darcy number 10^{-6} to 10^{-3}) and porosity values between $\varepsilon = 0.148$ and 0.887. Numerical simulations are carried out using a modified version of the `pimpleFoam` solver, while computational background cartesian mesh is generated using the OpenFOAM `blockMesh` utility. The case study aims to understand the influence of the Darcy number on drag coefficient characteristics and the underlying flow physics for stationary and rotating porous bodies. In the current study, only a one-way coupled fluid–structure interaction (FSI) approach is considered.

1 Introduction

Flow around porous bluff bodies is a fundamental problem in fluid dynamics with wide engineering applications, including heat exchangers, filtration systems, and biomedical equipment. The flow physics around bluff bodies and porous bodies are slightly different because in porous medium, a portion of fluid passes through porous body.

Henry Darcy, a chief site engineer for the piping system in the city of Dijon, France, introduced the basic physics of porous media. Darcy proposed that the pressure drop through a porous

medium is proportional to superficial velocity. Later, Forchheimer found that Darcy's law accurately represents the flow behavior at low velocities. However, at higher velocities, the pressure drop becomes nonlinear because inertial effects become significant.

At a low Darcy number (Da), the porous body behaves similarly to a solid body, allowing very little flow to pass through it. As Darcy number increases, more fluid passes through the porous medium, leading to changes in drag characteristics and a shortening of the wake region.

Numerical simulation of flow around bluff bodies is commonly performed using body-fitted meshes. However, generating body-fitted grids for complex or moving geometries can be computationally expensive and challenging. Therefore,Immersed boundary method (IBM) provides an efficient alternative by representing porous boundaries represented with non- dimensional term γ which represent porous volume fraction within a fixed Cartesian grid. IBM simplifies mesh generation and is particularly suitable for problems involving moving and rotating bodies.

In the current study, a one-way coupled fluid–structure interaction (FSI) approach is only studied. In one-way coupling, the fluid forces influence is studied as the motion of the rotating body, while the structural response does not affect the fluid solver through deformation feedback. Since the present work considers rotational motion without structural deformation, the one-way FSI framework provides an efficient and suitable approach for investigating wake behavior around the rotating porous square cylinder.

Among various porous bluff bodies, the square cross-section is considered in this study because it is one of the most widely studied geometries and has practical relevance in engineering applications. In the present work, flow in the *Re* range from $(10-40)$ is investigated. This range corresponds to the steady flow regime for the stationary case, where vortex shedding does not occur. However, for the rotating case, different behavior is observed. At Re = 40, the flow becomes unsteady and vortex shedding appears. Up to a certain rotational speed, vortex shedding is observed, but beyond that rotational speed, vortex shedding disappears and the flow becomes stable again.

The Darcy number (Da) represents the ratio of permeability of the square porous medium to characteristics length, i.e.,

$$\mathbf{Da} = \frac{k}{L^2} \tag{1}$$

Porosity(ε)represents the ratio of porous volume to total volume:

$$\varepsilon = \frac{V_P}{V} \tag{2}$$

The Reynolds number (Re) represents the ratio of inertial force to viscous force, i.e.,

$$\mathbf{Re} = \frac{\mathbf{UL}}{\nu} \tag{3}$$

2 Problem Description

The schematic representation of present computational domain is shown in Fig. 1. A porous square cylinder with a characteristic width W is subjected to a uniform incoming flow with a freestream velocity U_∞ within a confined domain. Appropriate Dirichlet and Neumann boundary conditions

are imposed sufficiently far from the cylinder to ensure computational feasibility while minimizing boundary effects. The fluid flow is assumed to be laminar and incompressible, and the effective viscosity of the fluid and the porous medium is considered equal ($\mu_f = \mu_p$). Furthermore, the porous cylinder is assumed to be structurally uniform, isotropic, homogeneous, and fully saturated with a single-phase fluid throughout the simulation.

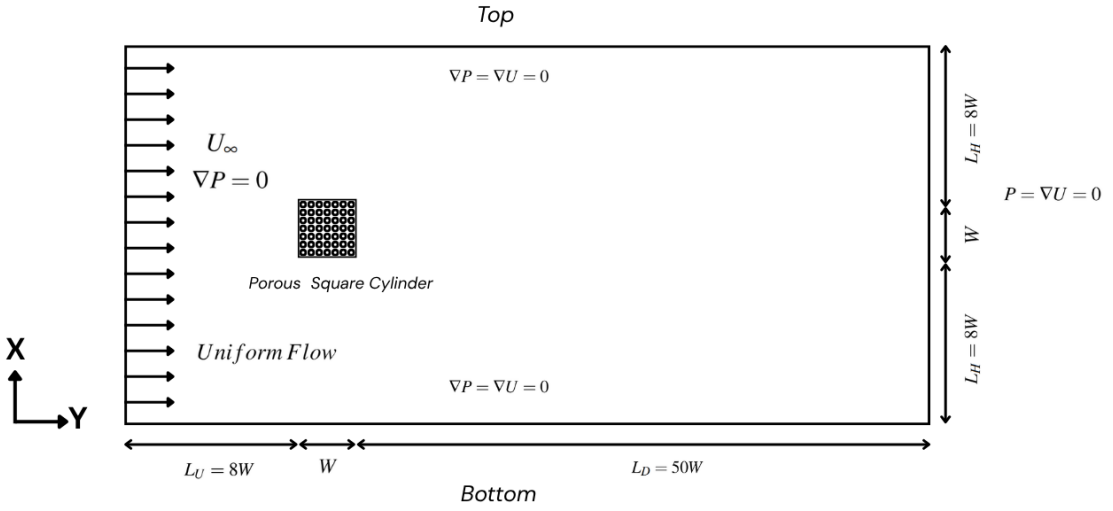

Figure 1: Geometry and domain dimensions

3 Solver, Governing Equations and Models

The modified pimpleFoam solver which implement a VARANS(Volume Average Reynolds Averaged Navier Stokes) equation to model a porous medium in fluid flow as in olaFLow and used continuous Forcing IBM(Immersed Boundary Method). Further, it has been modified,as per (Dhinakaran and Ponmozhi, 2011) for validation as per equation mentioned. As above assumption, fluid and porous region has been calculated using following equation:-

3.1 Mass Conservation (Continuity)

$$\frac{\partial}{\partial x_i}\frac{u_i}{n} = 0 \tag{4}$$

3.2 Momentum Conservation

3.2.1 Initial equation

$$\begin{aligned}\frac{1+c}{n}\frac{\partial}{\partial t}\frac{\rho u_i}{n} + \frac{u_j}{n}\frac{\partial}{\partial x_j}\frac{\rho u_i}{n} = &-\frac{\partial}{\partial x_i}p + \rho g_i + \frac{\partial}{\partial x_j}\left(\mu_e \frac{\partial}{\partial x_i}\frac{u_i}{n}\right) \\ &- a\frac{(1-n)^3}{n^2}\frac{\mu}{d_p^2}\frac{u_i}{n} - \frac{b\rho}{d_p}\frac{1-n}{n}\left(1+\frac{7.5}{KC}\right)\frac{u_i}{n}\left|\frac{u_i}{n}\right|\end{aligned} \tag{5}$$

3.2.2 Modified Equation

Momentum equation according to (Dhinakaran and Ponmozhi, 2011) for a porous model enforcing Darcy-Brinkman-Forchheimer model.

$$\rho\left(\frac{1}{n}\frac{\partial u}{\partial t}+\frac{u}{n}\frac{\partial u}{\partial x}+\frac{v}{n}\frac{\partial u}{\partial y}\right)=-\frac{\partial p}{\partial x}+\frac{\mu_e}{n}\left(\frac{\partial^2 u}{\partial x^2}+\frac{\partial^2 u}{\partial y^2}\right)-\frac{\mu}{\kappa}u-\frac{\rho F}{\sqrt{\kappa}}|\vec{V}|u \tag{6}$$

In above equation, $F=\frac{1.75}{\sqrt{150}}\frac{1}{n^{\frac{3}{2}}}$ is inertial factor and permeability $\kappa=\frac{1}{180}\frac{n^3 d_p^2}{(1-n)^2}$

Calculation:-

$$\frac{\mu}{\kappa}=180\frac{(1-n)^2}{n^3}\frac{\mu}{d_p^2} \tag{7}$$

$$\frac{\rho F}{\sqrt{\kappa}}=\frac{1.75}{\sqrt{150}}\sqrt{180}\frac{(1-n)\rho}{n^3 d_p}=1.917\frac{(1-n)\rho}{n^3 d_p} \tag{8}$$

Modified Momentum equation as used in solver which accurately mimic momentum equation based in (Dhinakaran and Ponmozhi, 2011), obtained from above calculation.

$$\begin{aligned}\frac{1+c}{n}\frac{\partial}{\partial t}\frac{\rho u_i}{n}+\frac{u_j}{n}\frac{\partial}{\partial x_j}\frac{\rho u_i}{n}=&-\frac{\partial}{\partial x_i}p+\rho g_i+\frac{\partial}{\partial x_j}\left(\mu_e\frac{\partial}{\partial x_i}\frac{u_i}{n}\right)\\&-a\frac{(1-n)^2}{n^2}\frac{\mu}{d_p^2}\frac{u_i}{n}-\frac{b\rho}{d_p}\frac{(1-n)}{n}\frac{u_i}{n}\left|\frac{u_i}{n}\right|\end{aligned} \tag{9}$$

Remark* The following governing equation is written in accordance with solver implementation in code.

3.3 Solver Setup

The modified `porousPimpleIbFoam` solver is based on a merger of the SIMPLE and PISO algorithms, along with a continuous forcing IBM implementation specifically designed for solving porosity-related problems.

3.3.1 Linear Solvers and PIMPLE Settings

The linear system for pressure is solved using GAMG (geometric algebraic multi-grid) solver with Gauss–Seidel smoother. Absolute tolerance of 1×10^{-6} and relative tolerance of 0.1 are used. For the final pressure corrector (`pFinal`) and the pressure corrector step (`pcorrFinal`),relative tolerance is set to 0 to enforce strict convergence. The velocity equations are solved with the `smoothSolver` (symmetric Gauss–Seidel). An absolute tolerance of 1×10^{-5} is applied for the predictor step (`U`), while the final corrector (`UFinal`) uses a tighter tolerance of 1×10^{-6}; no relative tolerance is employed in either case.

3.4 Numerical Schemes

Parameter	Discretization scheme	Order of accuracy
Time derivative	Euler	first order
Gradient	Gauss linear	second order
Divergence (convection, $\nabla \cdot (\mathbf{UU})$)	Gauss linearUpwind grad(U)	Second order
Divergence (viscous stress tensor)	Gauss linear	second order
Divergence (porosity-modified flux)	Gauss limitedLinearV1	second order (limited)
Laplacian	Gauss linear corrected	second order
Interpolation	linear	first order
Surface normal gradient	corrected	second order

Table 1: Discretization schemes and their orders of accuracy

4 Simulation Procedure

4.1 Geometry and Mesh

The background Cartesian mesh represent a 2D, rectangular domain of height = 8.5 and width = 29.5, extruded 0.1 in direction along z axis. The blockMesh utility tools is used for generation of non-uniform structural(hexahedral) mesh in computational domain. The rectangular computational domain is divided into 9 blocks and simple grading is used to cluster no of cells near a porous cylinder as owing to fact that flow phenomena near a fluid-porous interface required a special attention.

In x-direction, domain is split into three segment with left inlet zone (3.75 wide),middle zone(1 wide), and right outlet zone(24.75 wide).

In y-direction, domain is also split into three layer with bottom(4 high),middle(1 high),and top(4 high).

Parameter	Symbol	Value (m)	Description
Upstream length	L_u	4	Distance from inlet to the object/region
Square porous obstacle width	W	0.5	Width of the porous region
Downstream length	L_d	25.0	Distance from object/region to outlet
Height	H	8.5	Total height of the domain

Table 2: Geometry definitions of the background Cartesian mesh as in Fig. 1.

4.2 Creation of the Immersed Boundary (IB) Mask

This background Cartesian mesh is designed for the implementation of IBM, which helps capture a fine fluid–porous interface. A stereolithography (STL) file of a square cylinder with a fine

tri-surface structure is placed into the background mesh. IBM with continuous forcing and a cut-cell approach (similar to VOF) is used to define the IB mask using the following equation:

$$n_c = \gamma + n(1-\gamma) \tag{10}$$

where n is the porosity and γ is the VOF-like field defined as PVF $= V_{\text{subCell}}/V_{\text{cell}}$ (PVF stands for Porous Volume Fraction). V_{cell} is the volume of the cell, and V_{subCell} indicates the volume of the cell cut internally. Hence, inside the immersed body (the placed STL), $\gamma = 0$ and the porosity is the same as defined by the user. At the fluid–porous interface, the values of γ and porosity n vary between 0 and 1, and elsewhere they are defined as $\gamma = 1$ and $n = 1$.

4.3 Implementation of Rotation of the IB Mask

For rotating cases using the IBM approach, the background mesh cannot be changed at each runtime, as this would lead to high skewness and high computational cost. Rotating the IB mask is the ideal approach, but the value of the IB mask is defined based on the cut-cell approach. As the cylinder rotates about its center, new values of γ must be defined at every time step because the cut cells change. Therefore, we focus on rotating the STL file at every runtime at a prescribed angular speed ω. Since the STL file consists of many tri-surface points, each with a specific normal vector notation, Rodrigues' rotation formula is used to rotate the STL file at the prescribed ω. In the solver, the angle is defined as $\theta = \omega t$ (user-defined ω). At each time step, the angle θ is calculated from the user-defined rotation center and applied in Rodrigues' formula:

$$p_{\text{rot}} = p\cos\theta + (n \times p)\sin\theta + n(n \cdot p)(1-\cos\theta). \tag{11}$$

where, n is unit vector and p is a point on tri-surface of STL file.

The grid convergence/independence test is performed with three different grid size of $A(377 \times 154)$,$B(422 \times 191)$,and$C(505 \times 262)$ for finalizing the grid for simulation,which is detailed in section 5.1.The final converged mesh is display in Fig. 2.

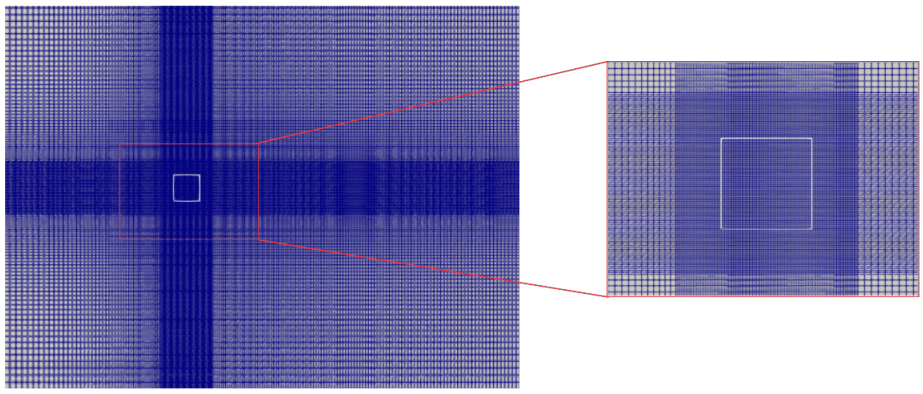

Figure 2: Background Cartesian mesh

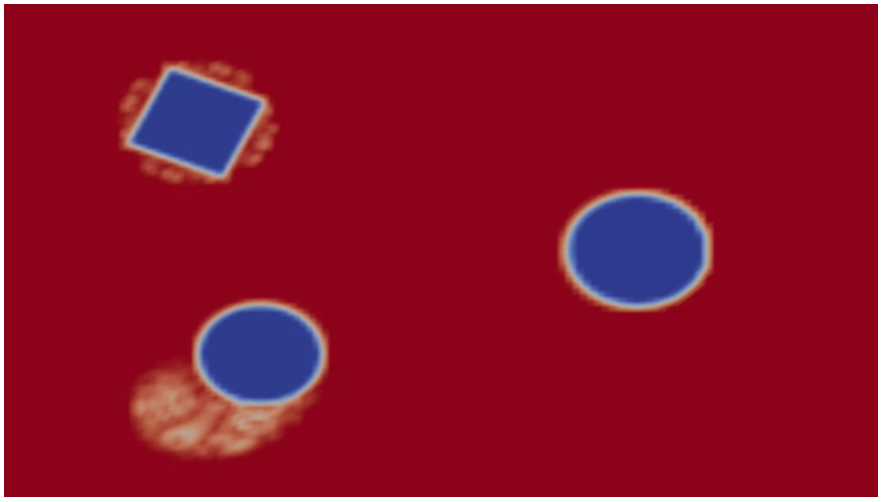

Figure 3: Rotation of a porous cylinder about its center and away from the center

4.3.1 Force Calculation

The total hydrodynamic force on the porous square cylinder is obtained by integrating the source term for porous medium over the volume where $\gamma < 1$:

$$\mathbf{F}_{\text{object}} = \int_{\gamma<1} \rho\, \mathbf{S}_{\text{porous}}\, dV.$$

The $C_D$and C_L coefficients are then defined as

$$C_d = \frac{F_x}{\frac{1}{2}\rho U_\infty^2 A_{\text{ref}}}, \qquad C_l = \frac{F_y}{\frac{1}{2}\rho U_\infty^2 A_{\text{ref}}},$$

with A_{ref} (projected area of porous cylinder) and U_∞ (free-stream velocity).

4.4 Initial and Boundary Conditions

Proper boundary conditions are required to perform an effective simulation. The boundary conditions for velocity and pressure on different walls and patches are as follows:

Boundary	Velocity (U)	Pressure (p)
Inlet	fixedValue; uniform (Ux 0 0)	zeroGradient
Outlet	zeroGradient	fixedValue; uniform 0
Top	symmetryPlane	symmetryPlane
Bottom	symmetryPlane	symmetryPlane
Front & Back	empty	empty

Table 3: Boundary conditions for the porous square cylinder case (2D).

Remark: The porous square cylinder is modeled via IBM and therefore does not require a patch definition.

4.5 Initial and Boundary Conditions

Proper boundary condition is required to perform a simulation in effective way. Hence boundary condition of Velocity and Pressure for different walls and Patch are as follow:-

Boundary	Velocity (U)	Pressure (p)
Inlet	fixedValue; uniform (Ux 0 0)	zeroGradient
Outlet	zeroGradient	fixedValue; uniform 0
Top	symmetryPlane	symmetryPlane
Bottom	symmetryPlane	symmetryPlane
Front & Back	empty	empty

Table 4: Boundary conditions for the porous square cylinder case (2D).

Remark* The porous square cylinder is model via the IBM and does not required to define and patch.

4.5.1 Initial Condition Calculation

Inlet Velocity Calculation for different Re.

$$Re = \frac{UL}{\nu} \tag{12}$$

Re	U_∞ (m/s)
10	0.002
20	0.004
30	0.006
40	0.008

Table 5: Free-stream velocity for different Reynolds numbers ($W = 0.5m$)

Calculation of Porosity(ε) **for different** Da

$$Da = \frac{\kappa}{W^2} \tag{13}$$

$$\kappa = \frac{1}{180}\frac{\varepsilon^3 d_p^2}{(1-\varepsilon)^2} \tag{14}$$

combining equation (7) and (8)

$$Da = \frac{1}{180}\frac{\varepsilon^3 d_p^2}{W^2(1-\varepsilon)^2} \tag{15}$$

Da	ε
1.0×10^{-6}	0.148
1.0×10^{-3}	0.715
1.0×10^{-2}	0.887

Table 6: Darcy number and corresponding porosity from the Carman-Kozeny relation ($d_p = 0.1$ m, $W = 0.5$ m)

Define value for coefficient a,b,c, and d.

Calculation:-

$$\frac{\mu}{\kappa} = 180\frac{(1-n)^2}{n^3}\frac{\mu}{d_p^2} \tag{16}$$

$$\frac{\rho F}{\sqrt{\kappa}} = \frac{1.75}{\sqrt{150}}\sqrt{180}\frac{(1-n)\rho}{n^3 d_p} = 1.917\frac{(1-n)\rho}{n^3 d_p} \tag{17}$$

where,

a	180
b	1.9
c	0
d_p	0.1

Table 7: value of coefficient a,b,c,and d_p

5 Results and Discussions

Simulations are performed in two phases: rotating and non-rotating cases. The simulation covers a Re range from $10 \leq Re \leq 40$ with a dimensionless Da range of $10^{-6} \leq Da \leq 10^{-2}$ for the non-rotating square porous cylinder. For the rotating square porous cylinder (rotation about its center), the rotational speed varies from $0.001 \leq \omega \leq 0.1$. The flow remains steady for all Reynolds numbers ($10 \leq Re \leq 40$); no Kármán vortex street is observed for any porosity value. However, when the porous square cylinder rotates at a certain angular speed, the Kármán vortex street begins to appear, specifically at $Re = 40$ and $Da = 10^{-3}$. As the rotation speed increases beyond a critical angular velocity ω_{critical}, the Kármán vortex street gradually fades, and the same trend is observed for high porosity values.

5.1 Mesh Independence Study

A grid convergence test was performed at $Re = 40$ and $Da = 10^{-3}$ to assess the dependence of the drag coefficient C_D on mesh resolution. The current solver was tested on three different grids of $X \times Y$ sizes: Grid A (377×154), Grid B (422×191), and Grid C (505×262), as shown in Table 8. The relative change in C_D from Grid B to Grid C is approximately 0.16%, which is well below the 1% threshold commonly accepted for grid independence. Considering both accuracy and

computational feasibility, Grid B (422×191) with a downstream length $L_D = 50W$ was selected for all subsequent simulations.

L_D	$\frac{C_D}{40}$
Grid A (377×154)	1.828
Grid B* (422×191)	1.836
Grid C (505×262)	1.839

**Selected grid for simulations.*

Table 8: Grid dependence test for C_D at $Da = 10^{-3}$

5.2 Validation

To validate the purpose numerical implementation using the continuous forcing IBM, the drag coefficient C_D for flow past a stationary porous square cylinder was compared with available literature values at different Re and Da. The validation was performed at $Da = 10^{-3}$ over the Reynolds number range $10 \leq Re \leq 40$. Table 5.2 presents a comparison of the present values with those reported by Dhinakaran and Ponmozhi (2011) and Anirudh and Dhinakaran (2018).

Re	Present	a	Dev. from a (%)	b	Dev. from b (%)
10	3.317	3.262	1.686	3.241	2.345
20	2.379	2.365	0.592	2.348	1.320
30	2.026	2.026	0.000	2.002	1.199
40	1.839	1.847	0.433	1.817	1.211

a: Dhinakaran and Ponmozhi (2011); b: Anirudh and Dhinakaran (2018).

Table 9: Comparison of drag coefficient C_D for $Da = 10^{-3}$: present values vs. references a and b.

The maximum deviation from reference a is 1.686% (at $Re = 10$), while the deviation from reference b is at most 2.345%. All deviations remain below 3%, confirming good agreement. The slight deviations may be attributed to differences in numerical schemes (the present solver employs a continuous forcing IBM, whereas the references used body-fitted grids) and the treatment of the porous interface. Overall, the validation demonstrates that the current solver is capable of accurately predicting the drag characteristics of porous square cylinders.

5.3 Effect of Da on Drag and Wake

The Darcy Number defined as $Da = k/D^2$, (where k is the permeability of porous medium and D is characteristics length of porous medium), quantifies importance of porous resistance over viscous effect. Fluid physics in which flow passing through a porous medium, drag coefficient and wake length exhibit strongly sensitivity toward value of porosity.

For low Darcy Number, the porous medium behaves as like a solid cylinder, which imposes high flow resistance and effectively there is formation of recirculation wake behind the body.

As the Darcy Number increase, the porous resistance weakens, allowing the flow pass through a porous medium and eventually drag coefficient decrease and there is slightly variation in wake length. As simulation is proceed for different Darcy Number,above mention phenomena is observed in simulation result as in Table 10.

Re	$Da = 10^{-2}$	$Da = 10^{-3}$	
	C_d	C_d	L_r
10	3.01	3.317	0.53
20	2.185	2.379	1.19
30	1.902	2.026	1.98
40	1.747	1.839	2.86

Table 10: C_d and L_r for different Reynolds numbers at two Darcy numbers (stationary case)

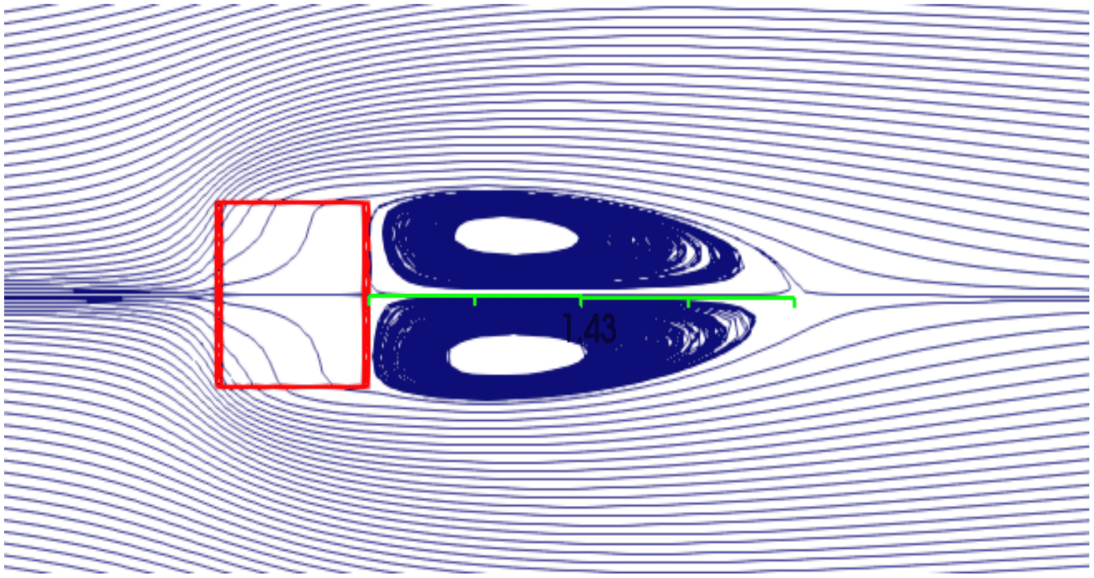

Figure 4: Vorticity pattern and recirculation length at $Re = 40$, $Da = 10^{-3}$

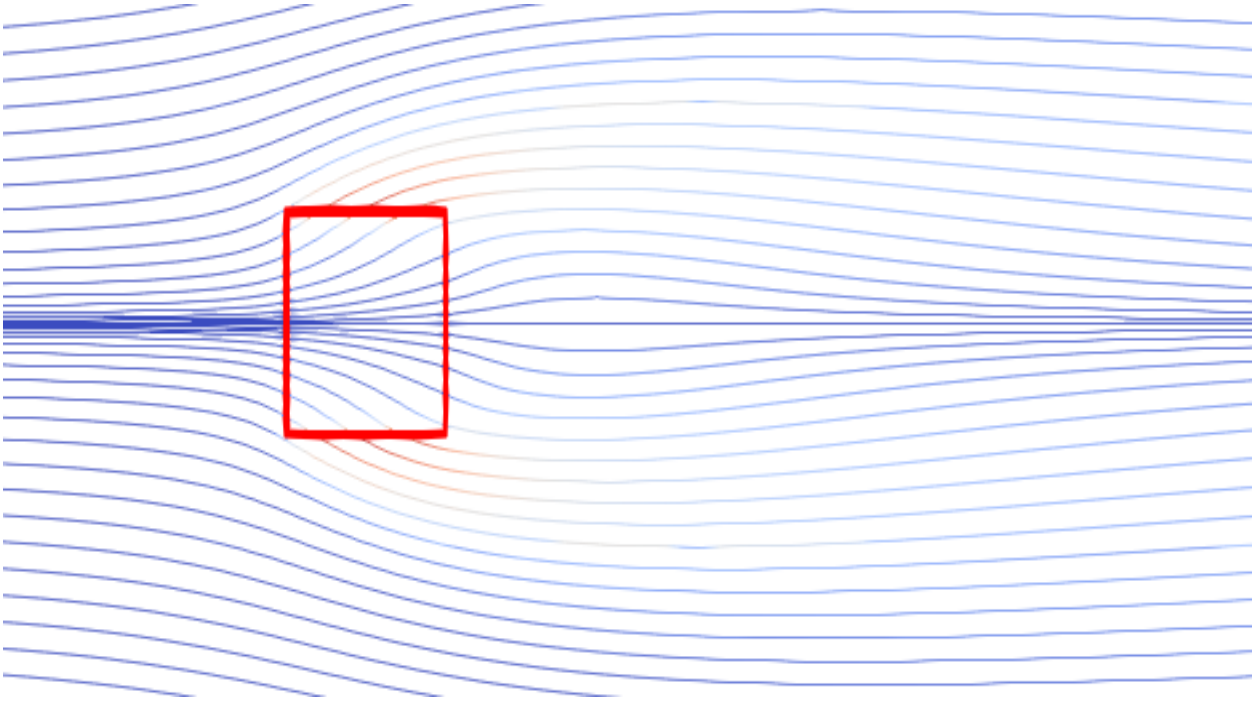

Figure 5: Vorticity pattern at $Re = 40$, $Da = 10^{-2}$

5.4 Effect of Rotation on Force Coefficients

To investigate the effect of rotation,simulation is performed for a porous square cylinder rotating about its center axis at different angular speed $(0.1 \leq \omega \leq 0.001)$ at different Reynolds Number keeping at $Da = 10^{-}3$.

For the non-rotating cylinder, flow is steady across all reynolds number ranging from $(10 \leq Re \leq 40)$ for different porosity value,i.e.; no Kármán vortex street was observed.

When rotation is imposed at $Re = 40$, the wake underwent a transition. At low angular speed, flow remained essentially steady. As ω increase about to 0.01, periodic vortex shedding appeared, a Kármán vortex street developed behind the cylinder as Fig 6.This is mainly cause due to magnus effect. Further increase in angular velocity beyond the critical angular velocity, vortex shedding fade, and flow eventually become steady. The root-mean square value and mean value of drag coefficient are reported in Table 5.4 for Reynolds Number $(10 \leq Re \leq 40)$ with three rotational rates and also a plot of C_l and C_d rms value while taking moving average of approx. 30 value is displayed in Fig. 8 to Fig. 13.

Re	$\omega = 0.1$		$\omega = 0.01$		$\omega = 0.001$	
	$C_{D,\text{rms}}$	$C_{L,\text{rms}}$	$C_{D,\text{rms}}$	$C_{L,\text{rms}}$	$C_{D,\text{rms}}$	$C_{L,\text{rms}}$
10	3.4481	0.0422	3.4182	0.0674	3.4033	0.0743
20	2.5589	0.0309	2.5215	0.0707	2.4634	0.1162
30	2.2029	0.0298	2.1582	0.0881	2.1018	0.0783
40	2.0224	0.0264	1.9701	0.0995	1.9219	0.0560

Table 11: $C_{d,\text{rms}}$ and $C_{l,\text{rms}}$ for different ω values at $Da = 10^{-3}$

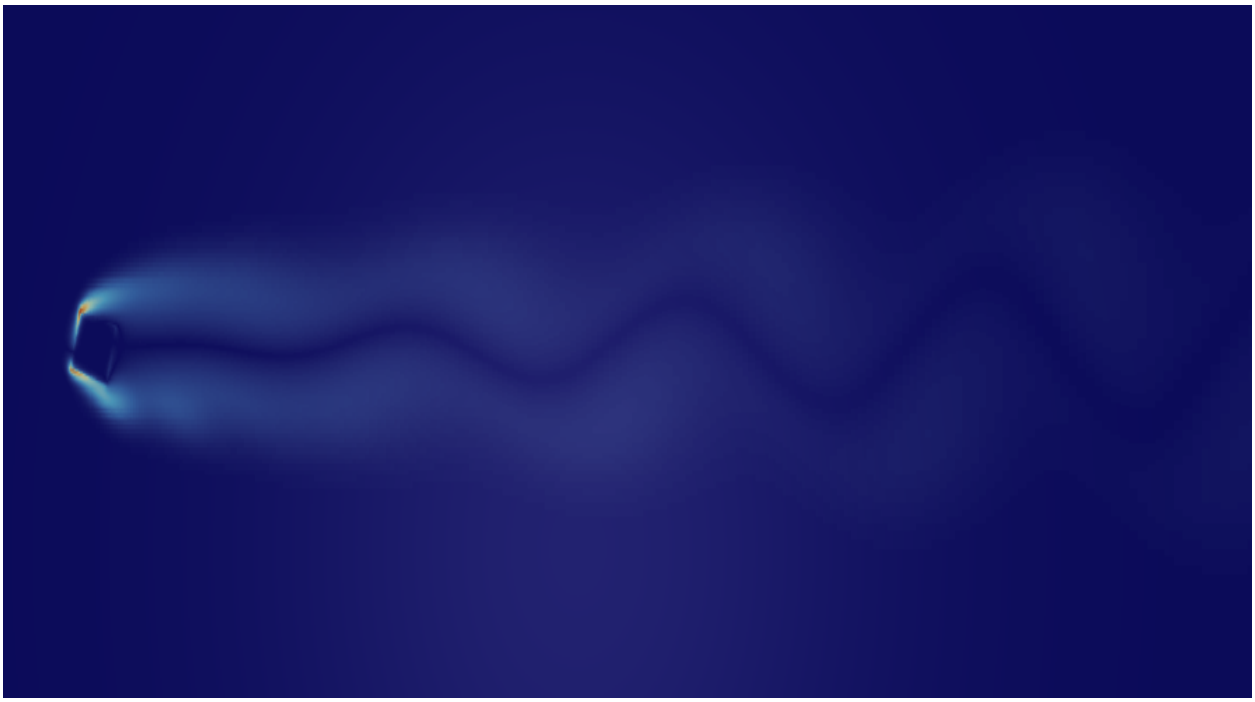

Figure 6: Unsteady flow pattern at $Re = 40$, $\omega = 0.01$, $Da = 10^{-3}$

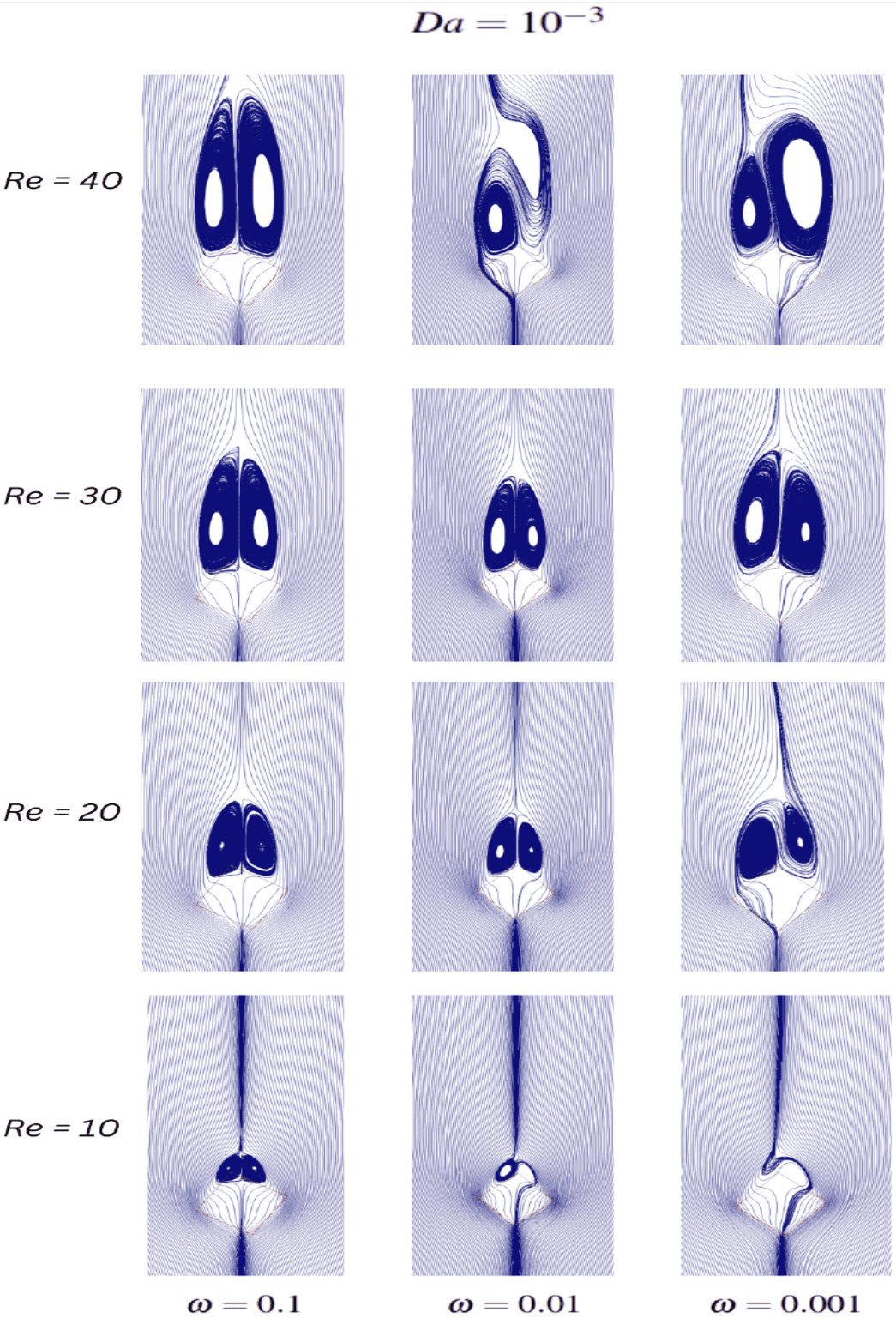

Figure 7: Streamline pattern of vorticity at different ω

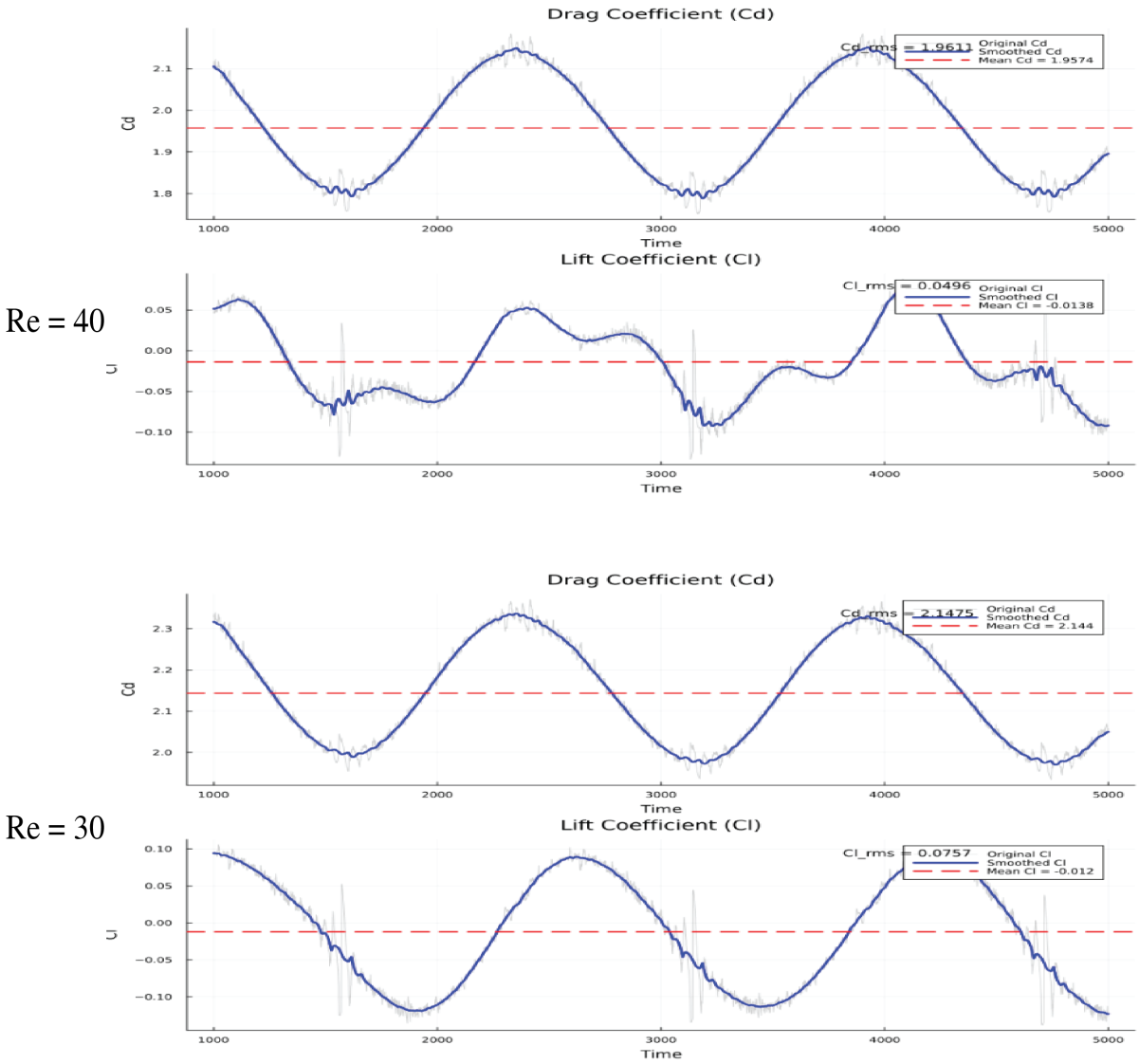

Ω=0.001

Figure 8: Moving average of C_D and C_L for $\omega = 0.001$

Re = 20

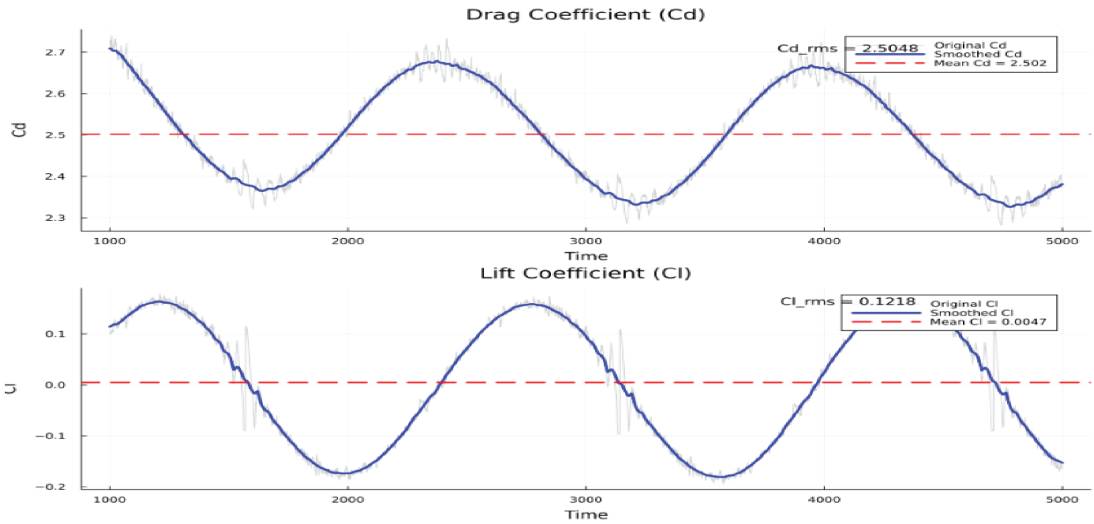

Re = 10

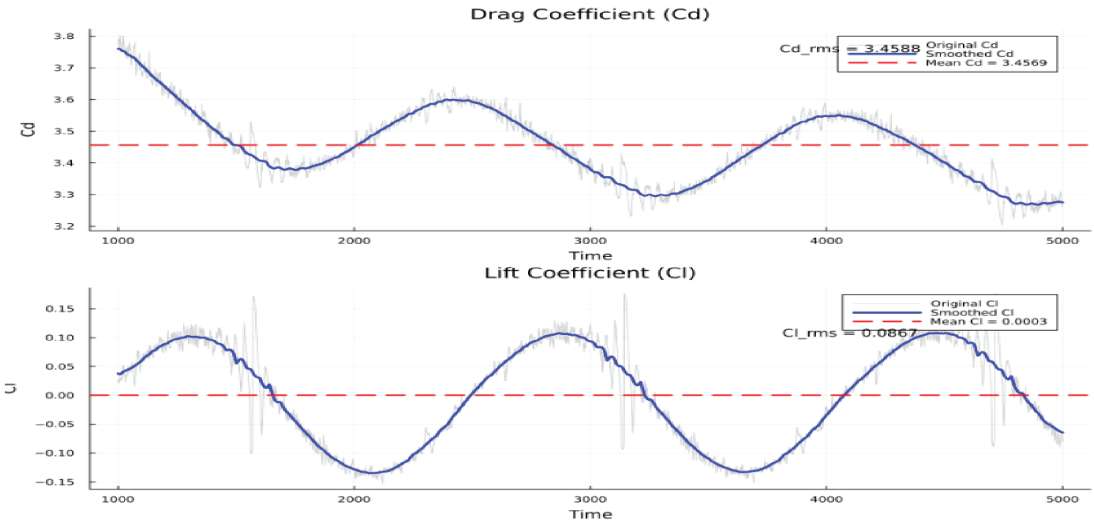

Ω=0.001

Figure 9: Moving average of C_D and C_L for $\omega = 0.001$ (continued)

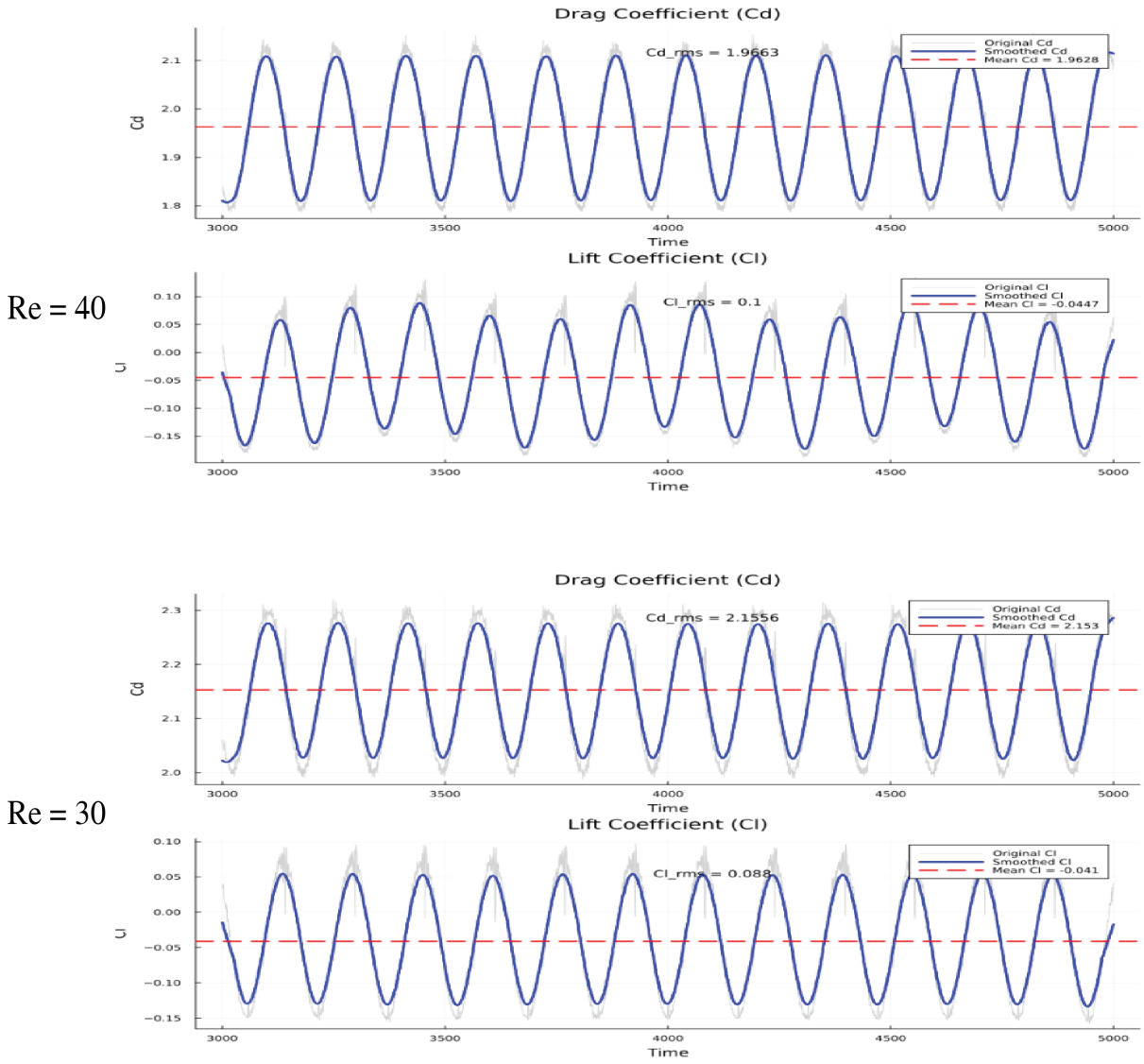

Ω=0.01

Figure 10: Moving average of C_D and C_L for $\omega = 0.01$

Re = 20

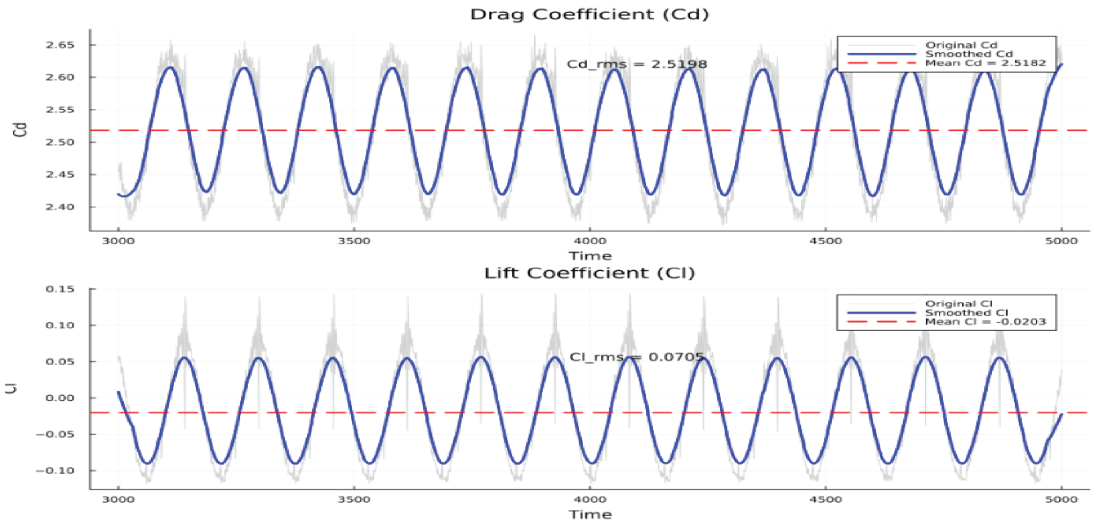

Re = 10

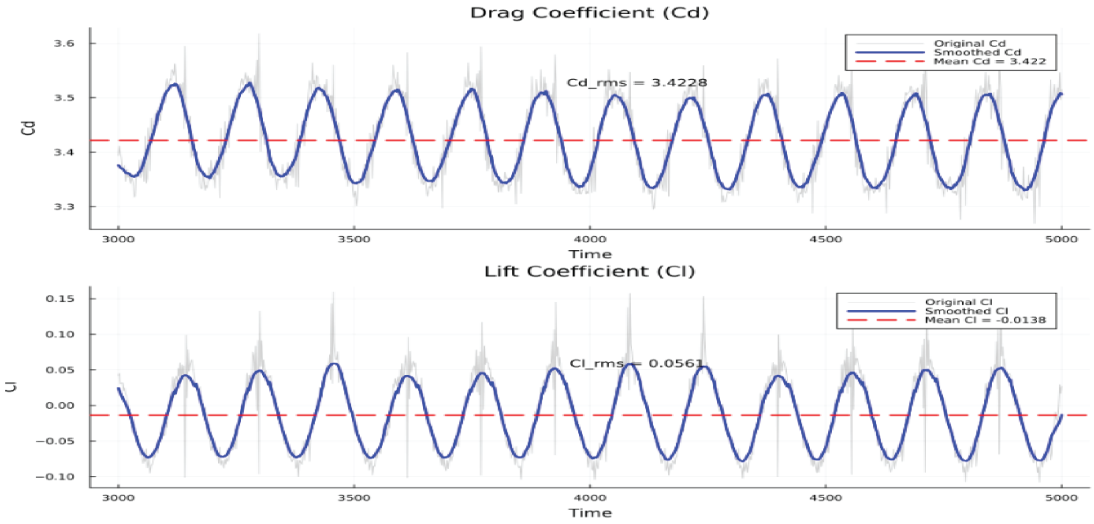

Ω=0.01

Figure 11: Moving average of C_D and C_L for $\omega = 0.01$ (continued)

Re = 40

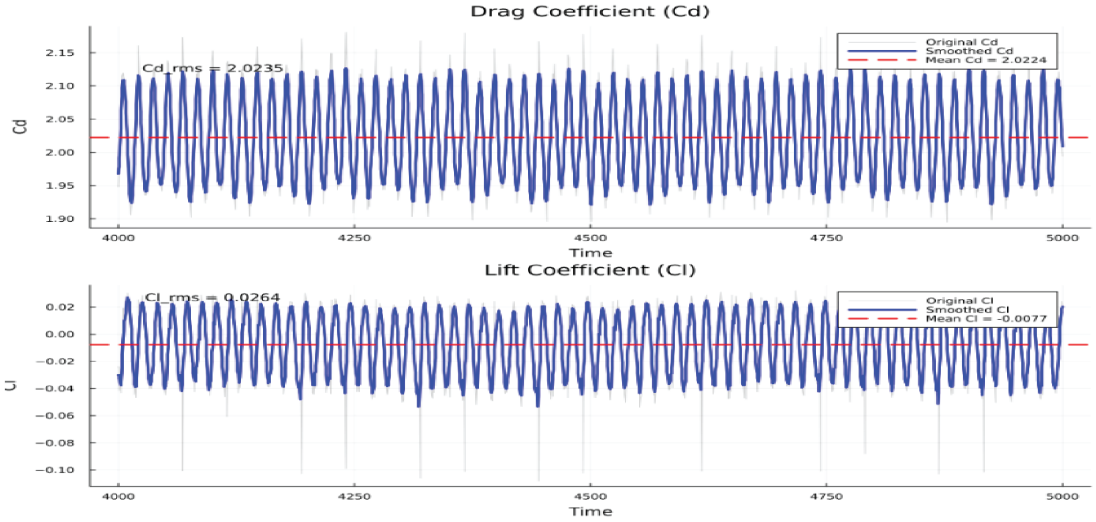

Re = 30

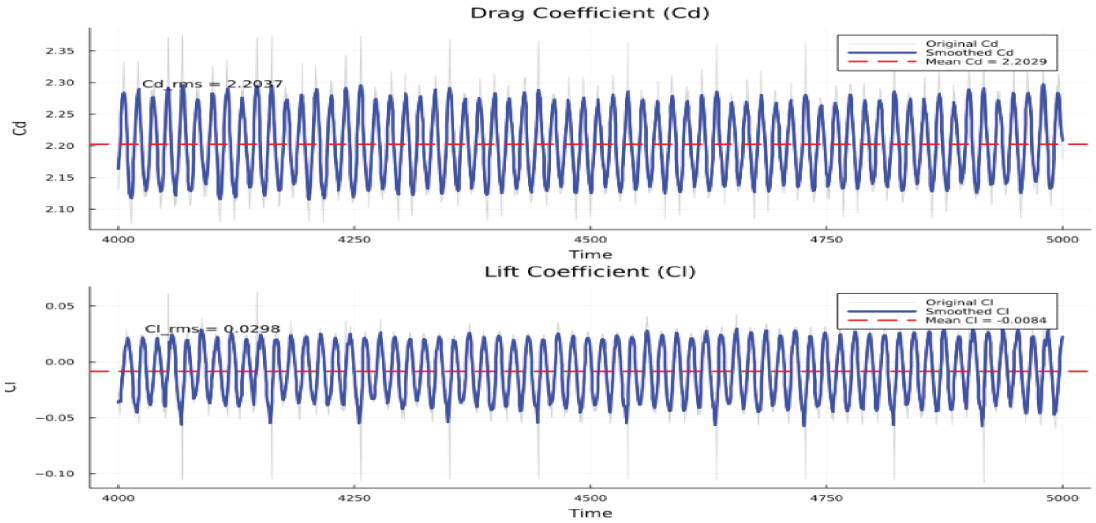

Ω=0.1

Figure 12: Moving average of C_D and C_L for $\omega = 0.1$

Re = 20

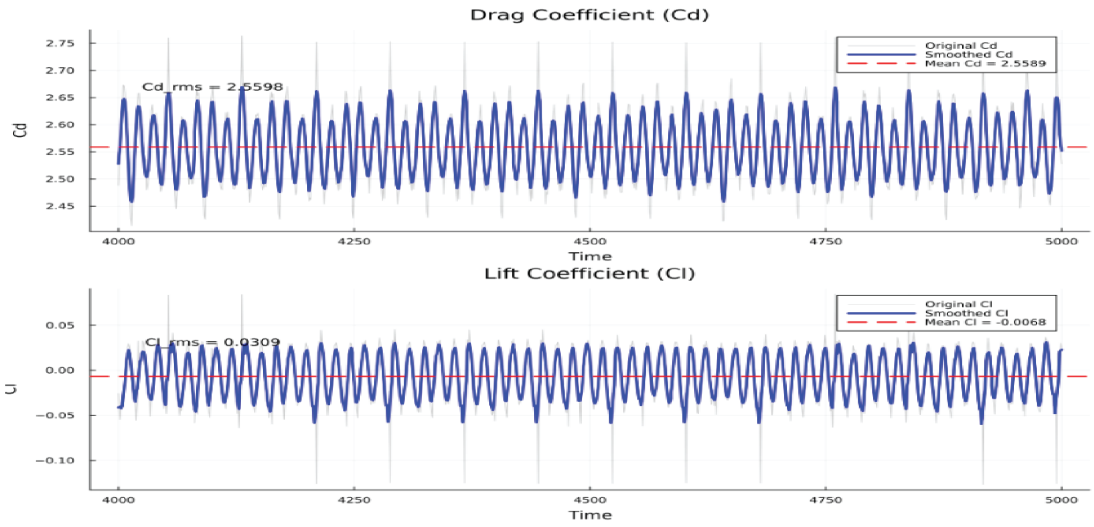

Re = 10

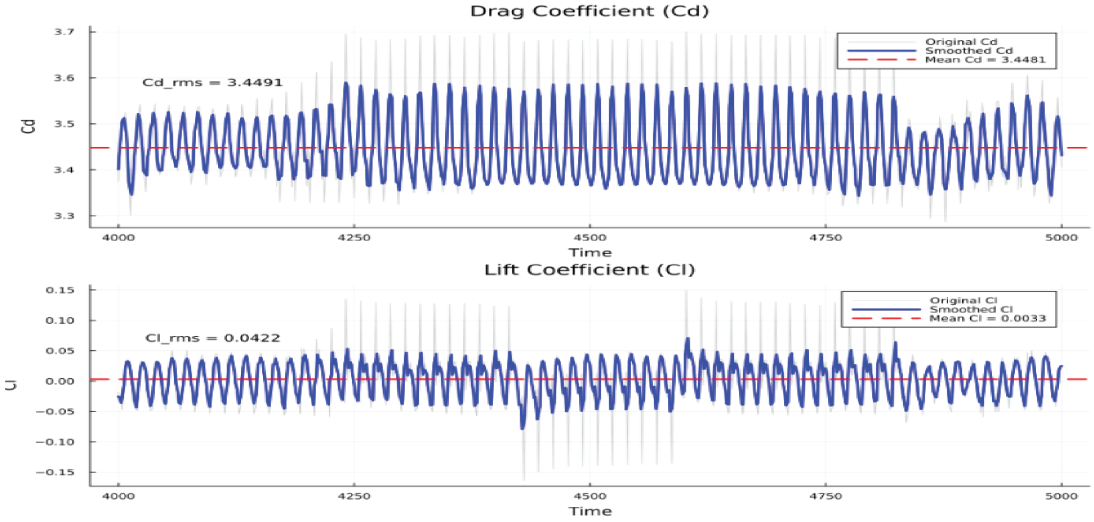

Ω=0.1

Figure 13: Moving average of C_D and C_L for $\omega = 0.1$ (continued)

6 Conclusion

The fluid dynamics of a 2D stationary and rotating porous square cylinder have been investigated in the present study. Numerical simulations for the steady regime in the Reynolds number range $10 \leq Re \leq 40$ with Darcy numbers 10^{-2} to 10^{-6} for the stationary case were performed. A grid independence study was conducted on three different grids (A, B, C), and Grid B was selected for simulation because the deviation of the drag coefficient from the finer Grid C was $\leq 1\%$.

Thus, Grid B was chosen for the simulation. The solver is a modified version of `pimpleFoam` and uses IBM to represent the porous cylinder without a conforming mesh. The accuracy of the solver was validated by comparing the drag coefficient for the stationary porous cylinder with reference data from the literature (Dhinakaran and Ponmozhi, 2011) and (Anirudh and Dhinakaran, 2018).

The present study focuses mainly on the rotating porous cylinder at three different angular speeds about its center (clockwise) at $Da = 10^{-3}$. Different flow patterns were obtained compared to the stationary case. Keeping the porosity constant, for a certain angular speed, swirling of the fluid was observed; as the speed increased further $\omega > \omega_{\text{critical}}$, the vortex patterns began to suppress, as noted in (Chatterjee and Gupta, 2015). A moving average using 20 nearest values was computed to determine $C_{d,\text{rms}}$. The obtained data for the rotating case are quite similar to the stationary case: as Re decreases, the drag coefficient increases.

References

Anirudh, K., and Dhinakaran, S. (2018). On the onset of vortex shedding past a two-dimensional porous square cylinder. *Journal of Wind Engineering and Industrial Aerodynamics*, 179, 200–214.

Chatterjee, D., and Gupta, S. K. (2015). Convective transport around a rotating square cylinder at moderate Reynolds numbers. *Numerical Heat Transfer, Part A: Applications*, 67(12), 1386–1407.

Dhinakaran, S., and Ponmozhi, J. (2011). Heat transfer from a permeable square cylinder to a flowing fluid. *Energy Conversion and Management*, 52(5), 2170–2182.